Isovector nuclear response in carbon

J. Ouyang,* S. Høibråten,† and R. J. Peterson
Nuclear Physics Laboratory, University of Colorado, Boulder, Colorado 80309-0446
(Received 3 September 1992)

The isovector nuclear response of carbon is calculated using a random-phase approximation technique for both the non-spin-flip and the spin-flip channel. The calculated results are found to be in fair agreement with experimental results from C(π^-,π^0) measurements at 500 and 400 MeV. The nuclear correlations quench and harden the charge-exchange quasifree peak as predicted.

PACS number(s): 25.80.Ls

I. INTRODUCTION

In a modern view, the nucleus is a collection of nucleons which interact with each other by exchanging mesons with a limited range of quantum numbers. This interaction for each spin and isospin channel can be studied indirectly by the corresponding nuclear response which can be obtained by quasifree (QF) projectile-nucleon scattering. In this paper, we assume that the interaction between the probe and the nuclear system can be described in two steps: first, the excitation, which is specific to the probe, and second, the propagation of this excitation within the nuclear system. The nuclear response, which corresponds to the second step, is the same for different probes. This two-step picture is essential for the discussions below.

A second assumption is that the loss of intensity for a strongly interacting beam can be treated by using an effective number of nucleons fewer than known for the target. For QF reactions, projectile-nucleus scattering can be understood in terms of projectile-nucleon scattering by introducing this effective number of nucleons and including nuclear medium effects. This allows us to factor the doubly differential cross section for a single scattering process in the laboratory frame as

$$\frac{d^2\sigma}{d\omega d\Omega} = N_{\rm eff} \sum_{\alpha} \frac{d\sigma}{d\Omega}\Big|_{\rm free}^{(\alpha)} S_\alpha(q,\omega) \ , \tag{1}$$

where ω is the energy loss, q is the laboratory momentum transfer, Ω is the solid angle, $N_{\rm eff}$ is the effective number of nucleons involved in the reaction [for (π^-,π^0) reaction, this is the effective number of protons], α corresponds to a channel of given spin and isospin, $d\sigma/d\Omega|_{\rm free}^{(\alpha)}$ is the singly differential cross section of the corresponding free projectile-nucleon scattering for channel α, and $S_\alpha(q,\omega)$ is the nuclear response for channel α.

In this presentation, we will compute the isovector nuclear response for the ^{12}C(π^-,π^0) reaction theoretically and compare these results to recent data, as analyzed specifically for comparison to the theory. In Sec. II we briefly present cross sections for the spin-flip and the non-spin-flip channels for free πN single charge exchange (SCX); in Sec. III we calculate the nuclear response using a random-phase approximation (RPA) technique, including appropriate relativistic kinematics; in Sec. IV we extract the nuclear response from our experimental data using the (π^-,π^0) reaction on carbon at beam energies of 500 and 400 MeV; in Sec. V we make a comparison between the theoretical and experimental results.

II. SINGLY DIFFERENTIAL CROSS SECTION FOR FREE πN SCX

For free πN SCX, the scattering amplitude can be expressed as

$$A(\theta_{\rm c.m.}) = f(\theta_{\rm c.m.}) + g(\theta_{\rm c.m.})\boldsymbol{\sigma}\cdot\hat{\mathbf{n}} \ , \tag{2}$$

where $\theta_{\rm c.m.}$ is the scattering angle in the πN center-of-mass (c.m.) frame, $\boldsymbol{\sigma}$ is the nucleon Pauli spin matrix,

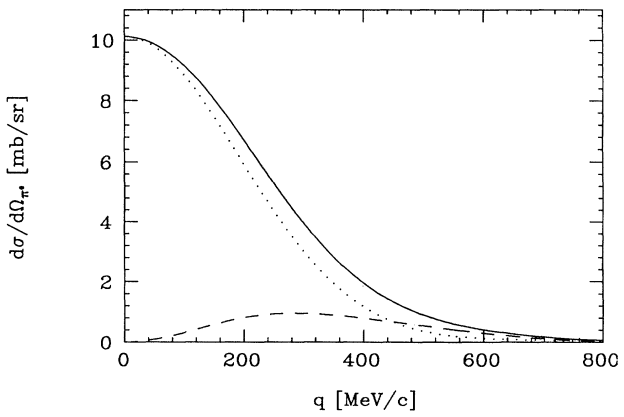

FIG. 1. The free πN SCX cross sections in the laboratory frame. The dotted line is the non-spin-flip singly differential cross section, the dashed line is the spin-flip cross section, and the solid line is the total cross section. The incident pion has a kinetic energy of 500 MeV. These curves are from phase-shift calculations [1].

*Present address: Physics Department, Boston University, Boston, MA 02215.
†Present address: Department of Physics, University of Virginia, Charlottesville, VA 22901.

$\hat{\mathbf{n}}$ is the unit vector normal to the scattering plane, and $f(\theta_{\text{c.m.}})$ and $g(\theta_{\text{c.m.}})$ are the non-spin-flip ($S = 0$) and the spin-flip ($S = 1$) complex amplitudes, respectively. The real and imaginary parts of both $f(\theta_{\text{c.m.}})$ and $g(\theta_{\text{c.m.}})$ can be found by the SAID program [1], which is based on phase-shift fits to πN scattering data.

As an example, non-spin-flip, spin-flip, and total πN isovector cross sections in the laboratory frame are shown in Fig. 1 for an incident pion energy at 500 MeV across the range of momentum transfers covered by the data. At small angles, the spin-flip cross section is small.

III. NUCLEAR RESPONSE FROM A THEORETICAL CALCULATION

We first introduce a random-phase approximation (RPA) framework for nuclear matter, then we give the important sum rule for a free Fermi gas, and we finally calculate the nuclear responses in ^{12}C for both the non-spin-flip and the spin-flip channel by using the concept of local nuclear matter.

A. Random-phase approximation

For nuclear matter, the response function for each channel α can be written as

$$S_\alpha(q,\omega) = -\frac{1}{\pi\rho}\text{Im}\Pi^\alpha(q,\omega) , \tag{3}$$

where $\Pi^\alpha(q,\omega)$ is the polarization propagator including all possible excitations for channel α, and ρ is the density of nucleons.

Since the important degrees of freedom for nuclear systems are limited to the nucleon and the Δ isobar for the nucleon spectrum at low and medium beam energies, the RPA expression for Π^α is

$$\Pi^\alpha = \frac{\Pi^0}{1 - v^\alpha_{ph}\Pi^0} , \tag{4}$$

$$\Pi^0 = \Pi^0_{ph} + \Pi^0_{\Delta h} , \tag{5}$$

where Π^0_{ph} and $\Pi^0_{\Delta h}$ are the noninteracting particle-hole (ph) and Δ-hole (Δh) polarization propagators which are independent of channels in nuclear matter, and v^α_{ph} is the ph interaction for channel α.

For the momentum transfers of our experiment where the nuclear isovector response is most interesting (from 256 to 661 MeV/c), Π^0_{ph} has to be calculated with relativistic kinematics, since the momentum of the recoil nucleon becomes comparable to the mass of a nucleon when the momentum transfer is high. However, for $\Pi^0_{\Delta h}$, we still simply use the nonrelativistic approximation since the mass of Δ is larger and $\Pi^0_{\Delta h}$ is much less important. Both Π^0_{ph} with relativistic kinematics and nonrelativistic $\Pi^0_{\Delta h}$ are given in the Appendix. Figure 2 shows an example for both the real and imaginary parts of Π^0_{ph} and $\Pi^0_{\Delta h}$. The peaks for the imaginary part are separated for ph and Δh, and this is true for all the momentum transfers in our experiment; the real part of $\Pi^0_{\Delta h}$ extends into the ph region; therefore $\Pi^0_{\Delta h}$ should be included when we do calculations for nuclear matter with interactions. For 256 MeV/$c \le q \le$ 661 MeV/c, the inclusion of Δh virtual process was found to bring the final QF peak of the response down (quench) and shift the peak to the lower energy loss (soften). This effect depends on the strength of ph interaction. At $q = 256$ MeV/c, where the interaction is important (see Sec. III C), the final QF peak of the response was found to be about 15% quenched and 2 MeV softened by the inclusion of Δh. At $q \ge 489$ MeV/c, where the ph interaction is small, the quench becomes less than 3% and the shift of the peak is less than 1 MeV.

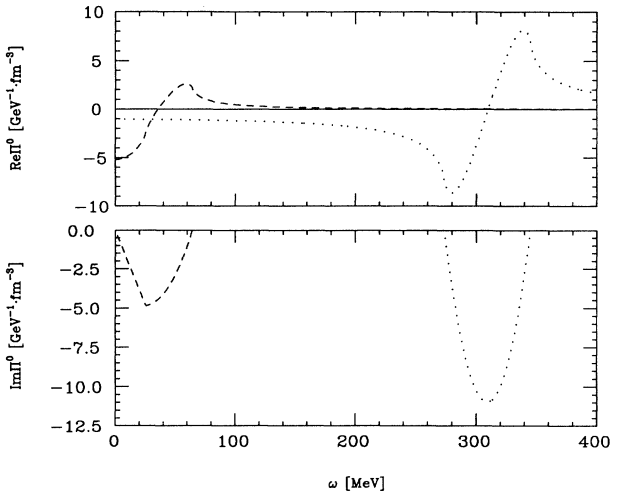

FIG. 2. Noninteracting polarization propagator. The dashed lines are for Π^0_{ph} calculated from Eqs. (A1) and (A4), and the dotted lines are for $\Pi^0_{\Delta h}$ calculated from Eq. (A10). Here, $p_F = 220$ MeV/c and $q = 200$ MeV/c.

From the expression of $\text{Im}\Pi^0_{ph}$ in the Appendix, the ph response region is within $0 \le \omega \le q$. This is where we will do calculations and compare to the experimental results. In this region, pion production is excluded, and the role in the response of the Δh in the nuclear medium is not large. This is the region of the response dominated by QF scattering.

B. Fermi gas without interaction

If there are no interactions between nucleons, each nucleon will respond individually, there will be no propagation of the excitation, and the response function for each different channel will be the same:

$$S^0(q,\omega) = -\frac{1}{\pi\rho}\text{Im}\Pi^0(q,\omega) , \tag{6}$$

where $S^0(q,\omega)$ is called the free response.

We now define a function $\lambda(m)$ as

$$\lambda(m) = \frac{\hbar}{mc} , \tag{7}$$

where m is in units of mass (SI unit), and λ is in units of

length. The density of nucleons for a Fermi gas can then be written as

$$\rho = \frac{2p_F^3}{3\pi^2\lambda^3(M)M^3} , \tag{8}$$

where p_F is the Fermi momentum, and M is the mass of a nucleon. In this presentation, all the masses, momenta, and energies are in units of MeV except where specially indicated. From above and the expression of $\mathrm{Im}\Pi^0_{ph}$ in the Appendix, the response function for the free Fermi gas with relativistic kinematics in the ph region is

$$S^0(q,\omega) = \frac{1}{qp_F^3}\left[\frac{1}{2}(E_F^3 - E_{\min}^3) + \frac{3}{4}\omega(E_F^2 - E_{\min}^2)\right] , \tag{9}$$

where E_F and $E_{\min}$ are defined in the Appendix.

The fraction without Pauli blocking is

$$P(q) = \int S^0(q,\omega)d\omega = \begin{cases} \frac{3}{4}\frac{q}{p_F}\left(1 - \frac{1}{12}\frac{q^2}{p_F^2}\right), & q \le 2p_F , \\ 1, & q > 2p_F . \end{cases} \tag{10}$$

The sum rule of Eq. (10) is also correct under a nonrelativistic approximation.

C. Nucleus with interactions

The response function has to be calculated for each channel when including the interactions between the nucleons, because the interactions are different for each channel (the non-spin-flip and the spin-flip channel for isovector pion SCX). Furthermore, the nuclear response for each channel can be different for each target nucleus. We need to use a finite nucleus instead of nuclear matter in the calculations.

The simplest way to calculate nuclear response for a finite nucleus is to introduce the concept of "local nuclear matter," which means that the nucleus can be treated as nuclear matter of appropriate density at any radius. For local nuclear matter at some radius r, Eq. (3) can be rewritten as

$$S_\alpha(q,\omega;r) = -\frac{1}{\pi\rho(r)}\mathrm{Im}\Pi^\alpha(q,\omega;r) , \tag{11}$$

where $\rho(r)$ is normalized to satisfy $\int \rho(r)d^3r = A$.

Unlike electron scattering where the total cross section is negligible, and the whole nucleus is homogeneously sampled (for a volume response), pion scattering samples the nuclear surface. The probability for the pion to sample the nucleus per unit radius will be proportional to

$$\frac{dP(r)}{dr} = C(r)4\pi r^2\rho(r) , \tag{12}$$

where $C(r)$, the local absorption factor, can be expressed through [2]

$$C^{1/2}(r) = \frac{1}{2}\int_{-1}^{1} dx \exp\left(-\sigma_{\pi N}^T \int_{-\infty}^{rx} dz\, \rho\{[r^2(1-x^2)+z^2]^{1/2}\}\right) , \tag{13}$$

where $\sigma_{\pi N}^T$ is the total cross section for πN scattering. $C(r)$ is shown in Fig. 3 for ^{12}C. The total nuclear response for channel α is an average of $S_\alpha(q,\omega;r)$ from the center to the surface weighted by the sampling probability, i.e.,

$$S_\alpha(q,\omega) = \int_0^{R_c} dr\, S_\alpha(q,\omega;r)\frac{dP(r)}{dr} \Big/ \int_0^{R_c} dr \frac{dP(r)}{dr} , \tag{14}$$

where R_c is the radius at the nuclear surface (see below). As in Ref. [3], the local density $\rho(r)$, local effective mass of a nucleon $M^*(r)$, and local Fermi momentum $p_F(r)$ are defined by the following equations:

$$M^*(r) = M[1 - \beta\rho(r)] , \tag{15}$$

$$\rho(r) = \frac{\rho_0}{1 + e^{(r-R_1)/a_1}} , \tag{16}$$

$$\frac{p_F^2(r)}{2M^*(r)} + W(r) = \frac{p_F^2(0)}{2M^*(0)} + W(0) , \tag{17}$$

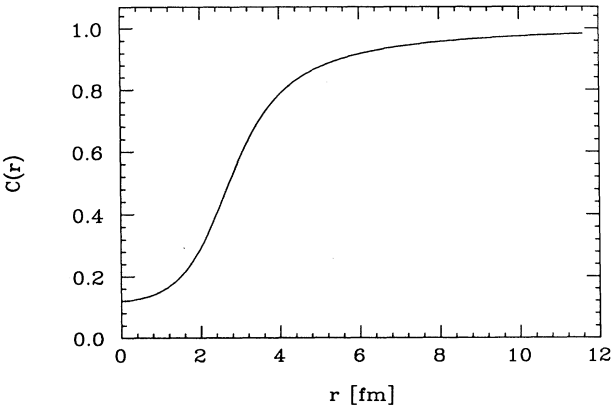

FIG. 3. The local absorption factor. This curve shows $C(r)$, with the total πN cross section of 26 mb which corresponds to pion scattering at 500 MeV for carbon.

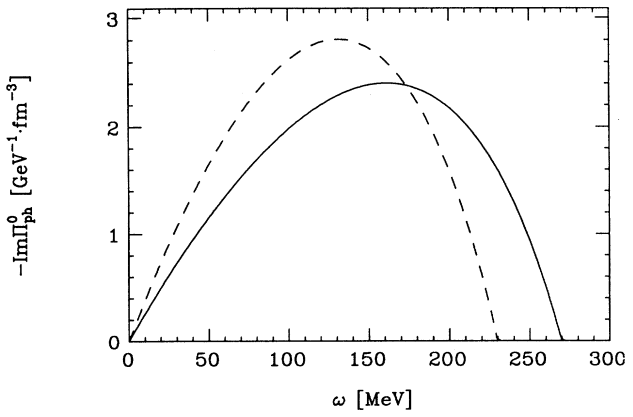

FIG. 4. The effect of the effective mass on nuclear response. For $q = 500$ MeV/c and $p_F = 250$ MeV/c, the dashed line is $-\mathrm{Im}\Pi^0_{ph}$ for the bare nucleon mass, and the solid line is $-\mathrm{Im}\Pi^0_{ph}$ for $\frac{M^*}{M} = 0.8$.

$$W(r) = \frac{V_0}{1 + e^{(r-R_0)/a_0}} \ . \tag{18}$$

All the parameters [β, ρ_0, $p_F(0)$, R_1, a_1, V_0, R_0, and a_0] here for ^{12}C are given in Ref. [3]. The radius at the nuclear surface (R_c) is defined by $p_F(R_c) = 0$.

Figure 4 shows $-\mathrm{Im}\Pi^0_{ph}$ as a function of the energy loss using the mass and a lower effective mass of a nucleon. The introduction of the lower effective mass is found to shift the QF peak of the response towards higher energy loss (harden) and bring the peak down (quench).

The inclusion of the local absorption factor $C(r)$ is found to soften and enhance the peak. This effect is similar to that for the effective mass, since the effective mass will increase as the scattering samples more of the nuclear surface [see Eq. (15)].

1. Non-spin-flip interaction

The non-spin-flip (π^-,π^0) isovector response is related to that for the "longitudinal" response in electron scattering, since both are driven only by the nuclear protons. The repulsive momentum-dependent ph interaction v^0_{ph} for the isovector channel is calculated in a semiclassical prescription with [3]

$$v^0_{ph}(r,q) = \Lambda^1(q) \frac{2\pi^2 \lambda^3 [M^*(r)]\, M^{*2}(r)}{p_F(r)} F_0^{0,1} \ , \tag{19}$$

$$\Lambda^1(q) = \left(\frac{\mu_1^2}{q^2 + \mu_1^2} \right)^{p_1} \ , \tag{20}$$

where $F_0^{0,1}$ is the isovector Landau parameter, and μ_1 and p_1 are the parameters entering into the form factor $\Lambda^1(q)$. The units used are the same as in Sec. III B. All the parameters here are given in Ref. [3].

Figure 5 shows v^0_{ph} as a function of radius at $q = 300$ MeV/c; the interaction is found to be repulsive everywhere. Figure 6 shows $\Lambda^1(q)$ as a function of momentum transfer across the range of q to be compared to the measurements below.

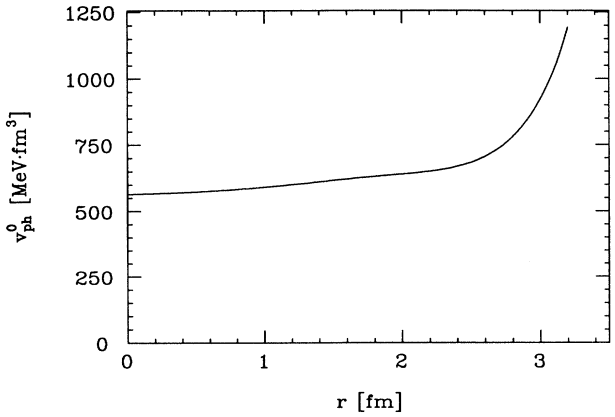

FIG. 5. The isovector interaction v^0_{ph} as a function of radius. This curve is calculated from Eq. (19). The momentum transfer is 300 MeV/c, and the target nucleus is carbon.

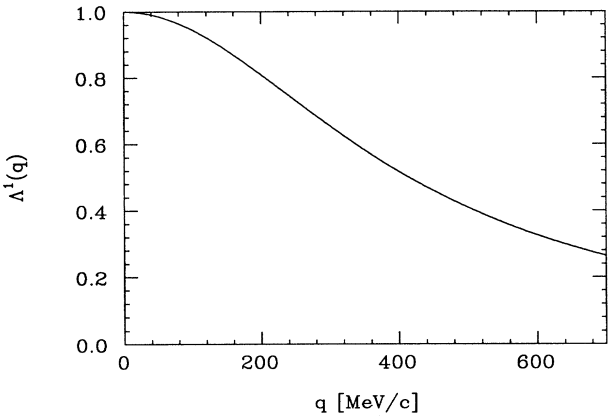

FIG. 6. Λ^1 as a function of laboratory momentum transfer. This curve is calculated from Eq. (20) with parameters for carbon.

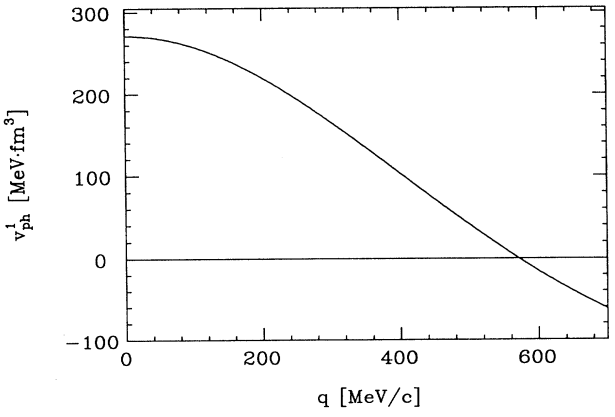

FIG. 7. The isovector interaction v^1_{ph} as a function of laboratory momentum transfer. This curve is calculated from Eq. (21). The energy loss is $\omega = 0$.

2. Spin-flip interaction

For pion SCX, we only have the transverse spin response because angular momentum and parity conservation exclude the longitudinal response for spin zero projectiles such as pions. The nonlocal ph isovector spin transverse interaction is [4]:

$$v^1_{ph}(q) = f^2_\pi \lambda^3(m_\pi) m_\pi \left(g' \Gamma^2_\pi - C_\rho \Gamma^2_\rho \frac{q^2}{q^2 + m^2_\rho - \omega^2} \right) , \tag{21}$$

where

$$\Gamma_\pi = \frac{\Lambda^2_\pi - m^2_\pi}{\Lambda^2_\pi - \omega^2 + q^2} , \tag{22}$$

$$\Gamma_\rho = \frac{\Lambda^2_\rho - m^2_\rho}{\Lambda^2_\rho - \omega^2 + q^2} . \tag{23}$$

Again, the units used are the same as in Sec. III B. The parameters take the values [4] $f^2_\pi/4\pi = 0.08$, $g' = 0.7$, $\Lambda_\pi = 1.3$ GeV, $\Lambda_\rho = 2.0$ GeV, and $C_\rho = 2.18$. The first term in v^1_{ph} is characterized by a short range repulsion, and the second term is from the exchange of a ρ meson with the approximation of zero width.

Figure 7 shows v^1_{ph} for the same range of q as in Fig. 6, covering the range of q spanned by the data to be shown in Sec. V. This spin-flip isovector interaction changes from strongly repulsive to weakly attractive across this range.

D. Average nuclear response

We define the average nuclear response as

$$\overline{S}(q,\omega) = \left[S_{S=0}(q,\omega) \frac{d\sigma_{(\mathrm{SCX})}}{d\Omega_{\pi^0}} \Big|^{(S=0)}_{\mathrm{free}} + S_{S=1}(q,\omega) \frac{d\sigma_{(\mathrm{SCX})}}{d\Omega_{\pi^0}} \Big|^{(S=1)}_{\mathrm{free}} \right] \Big/ \frac{d\sigma_{(\mathrm{SCX})}}{d\Omega_{\pi^0}} \Big|_{\mathrm{free}} , \tag{24}$$

where $S_{S=0}(q,\omega)$ and $S_{S=1}(q,\omega)$ are the nuclear responses for the non-spin-flip and the spin-flip channels, respectively, from above. $d\sigma_{(\mathrm{SCX})}/d\Omega_{\pi^0}|^{(S=0)}_{\mathrm{free}}$, $d\sigma_{(\mathrm{SCX})}/d\Omega_{\pi^0}|^{(S=0)}_{\mathrm{free}}$, and $d\sigma_{(\mathrm{SCX})}/d\Omega_{\pi^0}|_{\mathrm{free}}$ are the non-spin-flip, spin-flip, and total singly differential cross sections for free πN scattering, respectively. Both responses are calculated independently at each radius as for nuclear matter in Eq. (11) and then averaged from the center to the nuclear surface weighted by the local sampling probability as in Eq. (14).

IV. NUCLEAR RESPONSE FROM THE EXPERIMENT

$C(\pi^-,\pi^0)$ measurements with beams of 500 MeV and 400 MeV were performed at the High-Energy Pion Channel (P^3) at the Clinton P. Anderson Meson Physics Facility (LAMPF) using the π^0 spectrometer [5]. The scattering angles of the π^0 spectrometer were $\theta_{\pi^0} = 30°$, 50°, and 70° for 500 MeV π^-; 62.6° for 400 MeV π^- (this latter case attains the same momentum transfer as that for 500 MeV at 50°). Because the π^0 spectrometer measures a wide range of scattering angles around each central angle (θ_{π^0}), we chose three angular bins for the 500 MeV measurements, they are $\theta_{\pi^0} - 10.5°$ to $\theta_{\pi^0} - 3.5°$, $\theta_{\pi^0} - 3.5°$ to $\theta_{\pi^0} + 3.5°$, and $\theta_{\pi^0} + 3.5°$ to $\theta_{\pi^0} + 10.5°$. The three angular bins used at 400 MeV were selected to achieve the same momentum transfer at each end of the angular bin as that for the corresponding angular bin for the 500 MeV beam with $\theta_{\pi^0} = 50°$. The experimental data have been normalized to $H(\pi^-,\pi^0)$ [1] using a CH_2 target to match the carbon target. This experiment has also been described in Ref. [6].

The way to find the average nuclear response from the experimental results for each momentum transfer can be expressed as

$$\overline{S}(q,\omega) = \frac{d^2\sigma^{\mathrm{QF}}_{(\mathrm{SCX})}}{d\omega d\Omega_{\pi^0}} \Big/ \left(Z_{\mathrm{eff}} \frac{d\sigma_{(\mathrm{SCX})}}{d\Omega_{\pi^0}} \Big|_{\mathrm{free}} \right) . \tag{25}$$

Here $d^2\sigma^{\mathrm{QF}}_{(\mathrm{SCX})}/d\omega d\Omega_{\pi^0}$ is the measured QF doubly differential cross section. The QF peak is found on top of a smooth background in the spectrum for doubly differential cross sections. The extraction of the parameters (peak location, peak width, and the inclusive QF singly differential cross sections) of the QF peak for each angular bin was achieved by fitting the spectrum with an asymmetric Gaussian for the QF peak and a quadratic polynomial for the background (see Ref. [6], Ref. [7], or Ref. [8] for details). $d^2\sigma^{\mathrm{QF}}_{(\mathrm{SCX})}/d\omega d\Omega_{\pi^0}$ is the asymmetric Gaussian from this fit. Z_{eff} is the effective number of protons, which is extracted from the experiment. For $C(\pi^-,\pi^0)$, Z_{eff} is 2.79 ± 0.22 and 2.26 ± 0.48 for 500 MeV and 400 MeV beams, respectively [7]. $d\sigma_{(\mathrm{SCX})}/d\Omega_{\pi^0}|_{\mathrm{free}}$ is the singly differential cross section for free πN SCX which can be found from phase-shift calculations at both energies [1]. The background subtracted to give the single-nucleon response includes any nuclear response beyond the one-particle–one-hole.

V. COMPARISON BETWEEN THE THEORETICAL AND EXPERIMENTAL RESULTS

Figures 8–11 show both the experimental and calculated results. The data have been fitted with a peak above a smooth background due to processes other than those involving a single nucleon. For convenience in comparing the calculations, these fitted peaks are shown separately in the figures. The alternative method of adding the calculated responses to some empirical background could be compared to the actual data points shown. Since the fitting parameters are defined accurately by the wide range of energy loss, the fitted curves shown have small uncertainties to allow better comparisons to the computed responses.

At low momentum transfer (for example, q = 256 MeV/c) where nuclear correlations are important, the repulsive interactions for both the non-spin-flip

and the spin-flip channels produce strong quenching and hardening relative to the noninteracting calculation shown by the dotted curve. The width from the RPA calculation is found to be much narrower than that from the experimental data. This is because the energy resolution for our experiment is not included in the calculation. The large angular acceptance leads to a kinematic resolution of about 40 MeV for the free SCX peak on hydrogen. When added in quadrature to the solid line for the calculation in the figure at 256 MeV/c, the width observed for the heavy experimental fitted peak is nearly matched. The data reach their maximum at a higher energy loss than does the prediction at this low momentum transfer.

At moderate momentum transfer (for example, q = 437 MeV/c), the curve from the RPA calculation is found to be close to the noninteracting calculation because of the weak interaction. Both the width (since the width increases, the energy resolution become less important) and the position of the peak are in good agreement with our experimental data.

At high momentum transfer (for example, q = 584 MeV/c), there is almost no difference between the RPA and noninteracting calculations since the interaction almost vanishes for both the non-spin-flip and the spin-flip channels. When the momentum transfer is high, the relativistic effect becomes important; this effect softens and enhances the peak, compared to nonrelativistic calculations.

Data and calculations at a beam energy of 400 MeV are shown in Fig. 11, with the same momentum transfers as in Fig. 9 at 500 MeV. The average πN total cross section increases from 26.1 mb at 500 MeV to 29.1 mb at 400 MeV, making the reaction somewhat more concentrated in the surface at the lower energy. The parameters of the calculations that depend upon density were altered for the 400 MeV calculation and the different relative strengths of spin-flip and non-spin-flip scattering were included. At 400 MeV the continuum background is seen to be relatively more important. Comparison of Figs. 11 and 9 finds the same agreement between the data and the calculations at the two energies, using the fitted single nucleon peaks of the data.

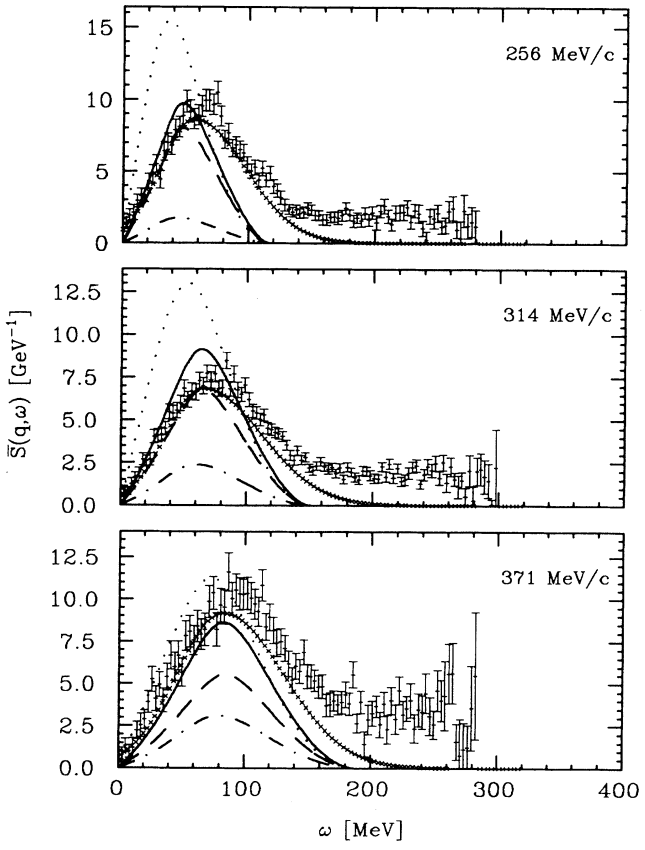

FIG. 8. RPA results for carbon at 30° with 500 MeV π^-. The line represented by the symbol × is the QF peak from the fit to the experimental data; the dotted line is the semiclassical calculation for free local nuclear matter; the dashed line is for the RPA non-spin-flip channel; the dot-dashed line is for the RPA spin-flip channel; the solid line is for the total RPA calculation. The corresponding momentum transfer is given in each plot.

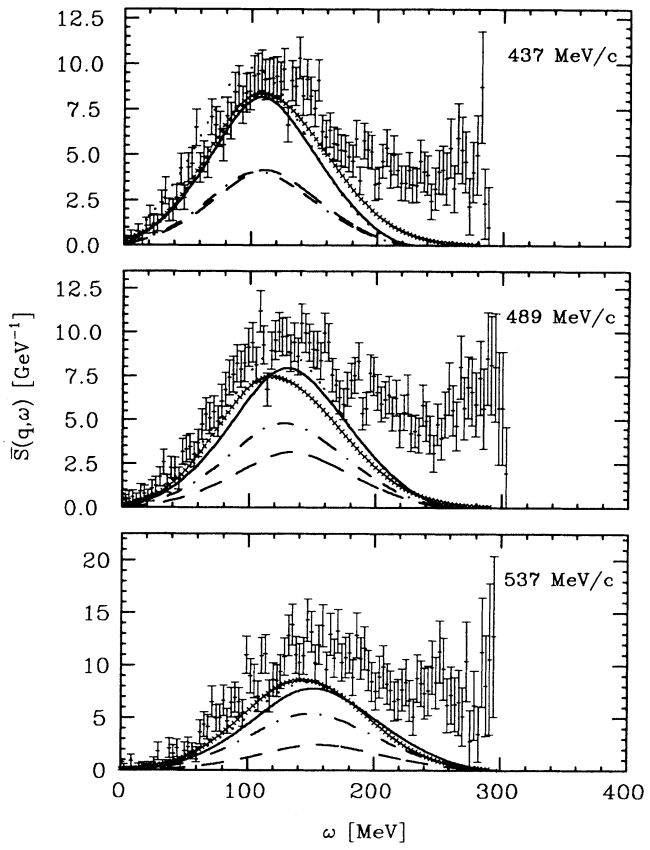

FIG. 9. RPA results for carbon at 50° with 500 MeV π^-. The line represented by the symbol × is the QF peak from the fit; the dotted line is the semiclassical calculation for free local nuclear matter; the dashed line is for the RPA non-spin-flip channel; the dot-dashed line is for the RPA spin-flip channel; the solid line is for the total RPA calculation. The corresponding momentum transfer is given in each plot.

Measured electron scattering charge responses of carbon are compared to RPA calculations for a similar range of momentum transfers in Ref. [3]. These are dominated at low q by the isoscalar response, not sensed by our charge-exchange reaction. The non-spin-flip response is shown in that work. The same trends of decreasing influences of nuclear interactions as q increases are shown in Ref. [3], and the general agreement between theory and experiment is comparable for electron scattering and pion SCX.

VI. SUMMARY AND CONCLUSIONS

We have examined the isovector nuclear response for both the non-spin-flip and the spin-flip channels over a large range of momentum transfers. We have improved and extended the theoretical framework built in Ref. [3] to isovector QF pion scattering. The differences are the following: (1) Relativistic kinematics are included. (2) The absorption factor for pion scattering is included. (3) The isovector spin transverse channel is examined. (4) Pion scattering enables us to avoid the need for a nucleon form factor, which was found to have to be renormalized in Ref. [3]. Since at lower momentum transfer (for example, $q = 256$ MeV/c), the singly differential cross section is dominated by the non-spin-flip channel (see Fig. 1), this work enables us to investigate an almost pure isovector non-spin-flip channel. We conclude that the collective effect produced from the repulsive ph interaction makes the QF peak quenched and hardened; the position, width, and cross section for the QF peak can be understood by this RPA framework.

ACKNOWLEDGMENTS

We thank the LAMPF staff for their support during the experiment, with special thanks to J. N. Knudson for his assistance with the π^0 spectrometer. We also thank M. R. Braustein, X. Y. Chen, W. Fong, E. R. Kinney, M. D. Kohler, J. J. Kraushaar, B. J. Kriss, D. J. Mercer, D. S. Oakley, D. L. Prout, R. A. Ristinen, and L. B. Weinstein for their help in running the experiment. D. L. Prout and J. R. Shepard are also thanked for helpful discussions about the theoretical part of this paper. This research was supported in part by the U.S. Department of Energy.

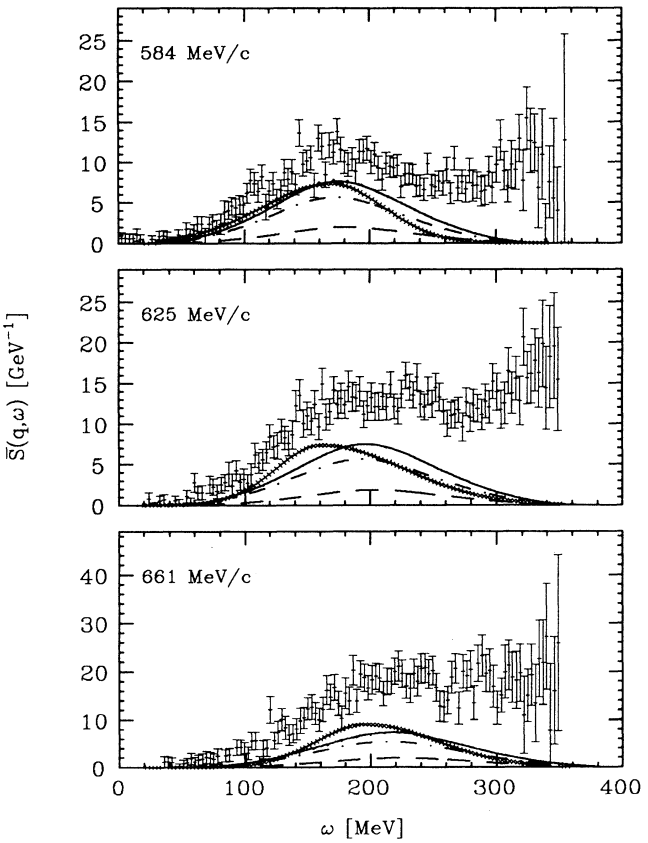

FIG. 10. RPA results for carbon at 70° with 500 MeV π^-. The line represented by the symbol × is the QF peak from the fit; the dotted line is the semiclassical calculation for free local nuclear matter; the dashed line is for the RPA non-spin-flip channel; the dot-dashed line is for the RPA spin-flip channel; the solid line is for the total RPA calculation. The corresponding momentum transfer is given in each plot.

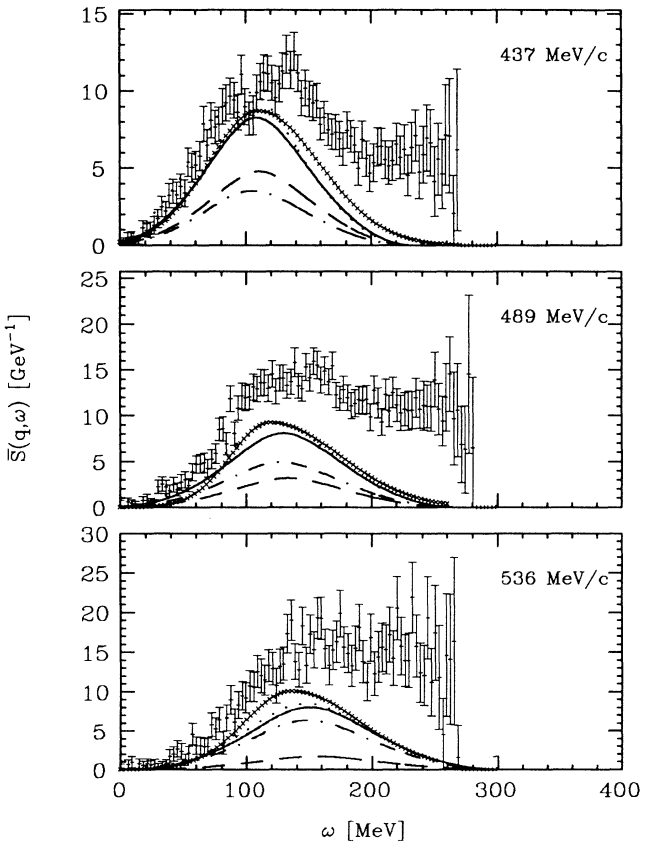

FIG. 11. RPA results for carbon at 62.5° with 400 MeV π^-. The line represented by the symbol × is the QF peak from the fit; the dotted line is the semiclassical calculation for free local nuclear matter; the dashed line is for the RPA non-spin-flip channel; the dot-dashed line is for the RPA spin-flip channel; the solid line is for the total RPA calculation. The corresponding momentum transfer is given in each plot.

APPENDIX: NONINTERACTING POLARIZATION PROPAGATOR

1. Π^0_{ph} with relativistic kinematics

We did the calculation for both the real and imaginary parts of Π^0_{ph} using relativistic kinematics. One integral is left for the real part since the integrand is quite a complicated function. For the imaginary part the deduction becomes much easier by using the notation given in Ref. [9]. The final results are

$$\mathrm{Re}\Pi^0_{ph}(q,\omega) = -\frac{2}{\pi^2\lambda^3(M)M^3}\int_M^{E_F} EdE\left(\frac{\xi_+ - \xi_-}{q} + \frac{\omega}{2q}\ln\left|\frac{\xi_+ - \omega - E}{\xi_- - \omega - E}\frac{\xi_- + \omega - E}{\xi_+ + \omega - E}\right| + \frac{E}{2q}\ln\left|\frac{\xi_+ - \omega - E}{\xi_- - \omega - E}\frac{\xi_+ + \omega - E}{\xi_- + \omega - E}\right|\right), \tag{A1}$$

$$E_F = \sqrt{p_F^2 + M^2}\,, \tag{A2}$$

$$\xi_\pm = \sqrt{(p \pm q)^2 + M^2}\,. \tag{A3}$$

For $\omega < q$,

$$\mathrm{Im}\Pi^0_{ph}(q,\omega) = -\frac{1}{\pi\lambda^3(M)M^3 q}\left[\frac{1}{3}(E_F^3 - E_{\min}^3) + \frac{1}{2}\omega(E_F^2 - E_{\min}^2)\right], \tag{A4}$$

$$E_{\min} = \min(E_F, E'_{\min})\,, \tag{A5}$$

$$E'_{\min} = \max(\eta, E_F - \omega, M)\,, \tag{A6}$$

$$\eta = \sqrt{\frac{M^2q^2}{q_\mu^2} + \frac{q^2}{4}} - \frac{\omega}{2}\,, \tag{A7}$$

$$q_\mu^2 = q^2 - \omega^2\,. \tag{A8}$$

For $\omega \geq q$,

$$\mathrm{Im}\Pi^0_{ph}(q,\omega) = 0\,. \tag{A9}$$

2. Nonrelativistic $\Pi^0_{\Delta h}$

The non-relativistic $\Pi^0_{\Delta h}$ is given in Ref. [10] as

$$\Pi^{0*}_{\Delta h}(q,\omega) = \frac{4p_F^2}{9\pi^2\lambda^3(M)M^3}\left(\frac{f_\Delta}{f}\right)^2\frac{1}{B^3}\left[B(A+A') + \left(\frac{B^2 - A^2}{2}\right)\ln\left(\frac{A+B}{A-B}\right) + \left(\frac{B^2 - A'^2}{2}\right)\ln\left(\frac{A'+B}{A'-B}\right)\right], \tag{A10}$$

where

$$B = \frac{q}{M_\Delta}\,, \tag{A11}$$

$$A = \frac{1}{p_F}\left(\omega - \omega_\Delta - \frac{q^2}{2M_\Delta}\right), \tag{A12}$$

$$A' = \frac{1}{p_F}\left(-\omega - \omega_\Delta - \frac{q^2}{2M_\Delta}\right), \tag{A13}$$

$$\omega_\Delta = M_\Delta - M_N\,, \tag{A14}$$

and f and f_Δ are the coupling constants for the πNN and $\pi\Delta N$ vertices, respectively. We use the Chew-Low relation $f_\Delta \approx 2f$, and neglect the width of the Δ which is hardly felt at the lower energy region.

[1] R. A. Arndt and L. D. Roper, Center for Analysis of Particle Scattering, Virginia Polytechnic Institute and State University, Report No. CAPS–80–3 (rev), 1983; R. A. Arndt, Z. Li, L. D. Roper, R. L. Workman, and J. M. Ford, Phys. Rev. D **43**, 2131 (1991).

[2] U. Stroth, R. W. Hasse, P. Schuck, W. M. Alberico, A. Molinari, and M. Ericson, Phys. Lett. **156B**, 291 (1985).

[3] W. M. Alberico, P. Czerski, M. Ericson, and A. Molinari, Nucl. Phys. **A462**, 269 (1987).

[4] W. M. Alberico, M. Ericson, and A. Molinari, Nucl. Phys. **A379**, 429 (1982).

[5] H. W. Baer, R. D. Bolton, J. D. Bowman, M. D. Cooper, F. H. Cverna, R. H. Heffner, C. M. Hoffman, N. S. P. King, J. Piffaretti, J. Alster, A. Doron, S. Gilad, M. A. Moinester, P. R. Bevington, and E. Winkelmann, Nucl. Instrum. Methods **180**, 445 (1981).

[6] R. J. Peterson, S. Høibråten, J. Ouyang, M. R. Braunstein, X. Y. Chen, M. D. Kohler, B. J. Kriss, D. J. Mercer, D. S. Oakley, D. L. Prout, and W. Fong, Phys. Lett. B **297**, 238 (1992).

[7] J. Ouyang, S. Høibråten, and R. J. Peterson, Phys. Rev. C **47**, 2809 (1993).

[8] J. Ouyang, Ph.D. thesis, University of Colorado, 1992.

[9] J. Shepard, Class Notes for Quantum Many-Body Physics, University of Colorado, 1992 (unpublished).

[10] E. Oset, *Spin Isospin Responses in Nuclei and Nucleons*, SERC Summer School, Jaipur, India, 1987 (unpublished).